Original Research

A Study on Biological Potential of PEG–Chitosan Dually Functionalized Silver Oxide Nanomaterials

Saman Ishfaq [1], Amna Bashir [1], Muhammad Khawar Abbas [2,*], Rimsha Aslam [1], Muhammad Azam [1], Syed Fazil Bin Farukh [1], Yasir Javed [1,*]

[1] Department of Physics, University of Agriculture Faisalabad, Faisalabad 38000, Pakistan;
[2] Department of Physics, Government College University Faisalabad, Faisalabad 38000, Pakistan
* Correspondence: Muhammad Khawar Abbas, m_khawarabbas@yahoo.com; Yasir Javed, myasi60@hotmail.com

Received: November 6, 2025; Accepted: February 24, 2026

Abstract: This study presented the synthesis of pristine, chitosan, and polyethylene glycol (PEG)–chitosan silver oxide nanoparticles (Ag_3O_4 NPs) using the hydrothermal technique and their potential for biological applications. Nano-systems were characterized via X-ray diffraction (XRD), UV-visible spectroscopy, Fourier transform infrared (FTIR) spectroscopy, and scanning electron microscopy (SEM). The average crystallite size of uncoated Ag_3O_4 NPs was 49 nm, and it is significantly reduced in the case of chitosan and PEG–chitosan conjugation, i.e., 25 nm and 22 nm, respectively. SEM micrographs indicated the spherical morphology of all three nano-systems. The chitosan and PEG–chitosan coating decreases the band gap of Ag_3O_4 NPs. Antibacterial potential was evaluated against *E. coli* and *S. aureus*. The antibacterial potential was enhanced after chitosan and PEG conjugation of Ag_3O_4 NPs. Chitosan-coated Ag_3O_4 NPs were more suited to radical scavenging for antioxidant properties, whereas *in vitro* alpha-amylase inhibition was most significant for PEG–chitosan Ag_3O_4 NPs.

Keywords: silver oxide; polymer functionalization; antibacterial; antioxidant; antidiabetic

1. Introduction

Metal oxide NPs have numerous uses in technology and medicine, and have received a lot of interest as antibacterial agents considering the increased bacterial resistance against prevailing antibiotics [1]. Although several antibiotics are available, resistance to nearly all of them has developed over time [2]. Silver's significant natural antibacterial properties against various pathogens, including bacteria, viruses, fungi, and yeast, are widely recognized [3]. The structural and redox characteristics, surface area-to-volume ratio, adjustable bandgap, exceptional dispersion, remarkable thermal stability, low volatility, and inherent biocompatibility of Ag_3O_4 NPs render them an ideal candidate for diverse biological applications, including wound healing, antibacterial, biofilm inhibition, antidiabetic, antioxidant, and antifungal properties, as well as anti-cancerous actions [4]. Silver oxide nanoparticles (Ag_3O_4) NPs offer added advantages over simple metallic silver NPs owing to the presence of mixed valence states of silver in the silver oxide structure, i.e., ($Ag^+/Ag^{2+}/Ag^{3+}$). This enhances redox action and generation of ROS [5]. In contrast to Ag NPs, which primarily rely on Ag^+ ions, Ag_3O_4 NPs yield sustained oxidative stress using lattice oxygen, consequently improving antimicrobial efficacy. It has been reported that Ag_3O_4 NPs possess superior photocatalytic and biocidal potential as compared to Ag_2O and Ag NPs due to a comparatively narrower band gap and higher surface reactivity [6]. Using steric repulsion, NPs can

be effectively protected against aggregation by covering their surface with layers of neutral organic molecules. By releasing Ag cations in a regulated manner, the distribution of silver NPs in a polymer matrix improves the antibacterial action and may significantly decrease the spread of infectious pathogens [7,8]. Ag cations are evenly distributed throughout the matrix, which inhibits particle aggregation whenever a composition of Ag_3O_4 NPs and a polymer is synthesized [9]. Polymers-coated Ag_3O_4 NPs additionally prevent bacteria from growing and reproducing on their surfaces [2]. Polymers, including PEG and chitosan, are used for coating NPs to extend their biocompatibility, therapeutic effectiveness, and antibacterial activity [10]. Furthermore, polymer films containing metal oxide NPs embedded in them and their surfaces contain antibacterial qualities [1,11].

PEG, a linear synthetic polymer, enhances the colloidal stability and biocompatibility of various metal oxide NPs for biological applications [12]. PEG has a neutral and hydrophilic nature. In addition, PEG coating reduces the harmful effects caused by potentially hazardous NPs. Chitosan, being relatively affordable to obtain from chitin, is the 2nd strongest natural biopolymer [13]. Chitosan-coated Ag_3O_4 NPs can achieve a dual function of an inorganic and organic component of the nanocomposite while being environmentally friendly, biocompatible, and possessing good antibacterial properties [14]. Chitosan-coated Ag NPs can also eliminate gram-negative (G−) and gram-positive (G+) bacteria and fungi [15]. Laib et al. [16] found strong antibacterial activity of ciprofloxacin-loaded silver NPs with the highest inhibition zone of 34 mm for *B. subtilis* and *K. pneumonia*. The synergy was observed due to the effects of ciprofloxacin in inhibiting DNA gyrase and ROS production with Ag NPs and membrane damage, which allowed the enhanced action against G+ and G− bacteria. Qadeer et al. [17] observed that PEGylated Ag NPs have shown higher antioxidant activity (128.72 ± 3.12 μg/mL) than pristine Ag NPs. Similarly, PEG-capped $Ni_xCo_{1-x}Fe_2O_4$ nanocomposites presented moderate antimicrobial properties and increased antioxidant/antidiabetic properties with PEG functionalization. PEG-coating increased total phenolic content (15.9 to 19.3 μg GAE/mg) and flavonoid content (8.7 to 9.3 μg QE/mg), DPPH scavenging (32.2% to 39.1%), and total antioxidant capacity (17.9 to 18.8 μg AAE/mg), which was attributed to the carbonyl/ester groups' presence in PEG [18]. Rajkumar et al. [19] studied PEG-coated CuO nanocomposites, which showed good antioxidant, antibacterial, and antidiabetic properties. The nanocomposites were found to have a strong DPPH scavenging (81.65% ± 1.65% at 100 μg/mL, IC_{50} (73.02 μg/mL), ABTS (70.58% ± 1.27%), and H_2O_2 (77.82% ± 1.25% at 100 μg/mL) scavenging power.

A conflict between the system and the generation of free radicals that protects against them is known as oxidative stress. Different types of triggered oxygen that lead to lipid peroxidation and the potential for inflammation are known as reactive oxygen species (ROS) [20]. Increased phagocyte activation and free radical generation in numerous inflammatory diseases lead to changes in membranes, protein denaturation, and vascular permeability. Because of this, anti-inflammatory or antioxidant drugs are required to reduce inflammation and oxidative stress. Several synthetic antioxidants are presently in use and commercially available; however, because of their toxicity and potential health risks, there is a greater need for natural antioxidants [21]. Therefore, research is being done on novel antioxidants that don't have toxic effects. In the current research work, the surface of Ag_3O_4 NPs is dually functionalized with PEG and chitosan polymers using the hydrothermal method. Dual coating synergizes the steric stabilization ability of PEG (due to its hydrophilic and slightly neutral nature) with the cationic bio-adhesion characteristics of

chitosan. This combination (PEG–chitosan) boosts colloidal stability, bioavailability, biocompatibility, and better bacterial membrane adsorption of nanomaterials. In the case of single coating, chitosan-coated NPs may aggregate in biological media, whereas PEG lacks mucosal adhesion at times. Dual coating can improve the stability of Ag_3O_4 NPs by overcoming these limitations. Moreover, chitosan disrupts bacterial membrane and PEG prolongs retention time, thus demonstrating good synergistic antibacterial activity. Additionally, chitosan enables pH-based release of silver ions while PEG minimizes opsonization. These physicochemical reactions signify the dual functionality of Ag_3O_4 NPs with PEG and chitosan [22–24]. The materials were characterized by using XRD, FTIR, SEM, and
UV–Vis spectroscopy. The two-fold coated Ag_3O_4 NPs were tested for their antibacterial, antidiabetic, and antioxidant properties.

2. Materials and methods

2.1. Materials

Silver nitrate ($AgNO_3{\cdot}6H_2O$, DAEJUNG Korea), Sodium hydroxide (NaOH, Icon Chemicals, India), PEG-6000 (DAEJUNG Korea), and Chitosan (Icon Chemicals, India) were used to prepare nanomaterials and functionalize them.

2.2. Synthesis of dually functionalized Ag_3O_4

Silver oxide NPs (Ag_3O_4 NPs) were synthesized using the hydrothermal method, where a 1:4 molar ratio of $AgNO_3{\cdot}6H_2O$ to NaOH was used for maintaining alkaline conditions (pH ~10), which facilitates the formation of Ag(III) species [25,26]. The 0.25M (4.25 g) of silver nitrate and 1M (4 g) of NaOH were dissolved separately in 100 mL of distilled water. NaOH (1 M) solution was added drop by drop to the silver nitrate solution. The pH was maintained at ~10 and stirred at 500 rpm for 2 h before hydrothermal treatment. The solution was put into a Teflon-lined autoclave and thermally heated in an oven at 180 °C for 16 h. Later, the precipitates were processed by centrifugation and rinsed with distilled water thrice to eliminate by-products and contaminants. The retrieved precipitates were put for drying in an oven at 60 °C and subsequently homogenized into a powder form. For functionalization, 0.1 g of each chitosan and PEG-6000 was added before incorporating the NaOH solution, and the same steps were followed as discussed for the preparation of pristine Ag_3O_4.

2.3. Characterization tools

The structural study was performed using XRD with a D8 Advance Bruker instrument. The analysis was performed between the 2-theta range of 20° to 60°. The SEM (NOVA NanoSEM) was utilized for morphological assessment. The Agilent Technologies Cary 630 FTIR instrument was utilized to validate the presence of functional groups. The optical characteristics were investigated using a UV–Vis spectrophotometer (PG Instrument, T80).

2.4. Antibacterial assessment

The nutrient agar (28 g) was mixed thoroughly in distilled water (1000 mL) in a flask. The solution was sterilized at 121 °C for 15 min by autoclaving. The temperature of the flask was checked by placing a thermometer. The temperature was 80 °C in the beginning and reduced to 40 °C after
75 min. The bacterial strain (0.16 mL) was added to the prepared medium. After that, wells were made with the help of a pipette tip, and 0.1 mL sample solutions were loaded in the wells on the growth medium, while the antibiotic, Ciprofloxacin, was also added in the central well as a positive control. The prepared Petri plates were kept in an incubator for 24 h at 37 °C, and clear zones were

formed. Conditions: Triplicate wells per sample, 0.1 mL of 1 mg/mL NP dispersion, Positive control (ciprofloxacin, 10 μg/mL), Negative control (sterile water).

2.5. Antioxidant assay

The antioxidant properties were studied on the 2,2-Diphenyl-1-picrylhydrazyl (DPPH) assay to assess the free radical scavenging capacity of functionalized Ag_3O_4 at the specific concentration of 10 mg/mL. Ascorbic acid (0.1 mg/mL) was used as a positive control to incorporate positive variations in DPPH activity. In 96-well plates, a previously established methodology (Mustafa et al. [27]),
0.01 mL of prepared solution in methanol (Concentrations: 2.12, 4.25, 6.37, 8.5, and 10 mg/mL) was combined with 0.5 mL of 0.2% DPPH solution. After 1 h incubation in the dark, the optical density was measured in the form of absorbance at 517 nm to ascertain the percentage of scavenging capacity of the tested materials using Equation (1).

$$\text{DPPH Inhibition (\%)} = \frac{Abs^{b} - Abs^{s}}{Abs^{b}} \times 100 \quad (1)$$

where Abs^{b} and Abs^{s} represented the absorbance of the blank and sample, respectively.

2.6. Antidiabetic assay

The alpha-amylase inhibition experiment, as specified by Zohra et al. [28] with minor modifications, was implemented to evaluate the potential of Ag_3O_4 NPs as an antidiabetic drug. To produce the reaction mixture, 0.01 mL of test samples (dilution concentration of prepared-NPs ranging from 200 ppm to 800 ppm), 0.015 mL of PBS (pH 6.8), 0.04 mL of starch solution, and 0.025 mL of alpha-amylase enzyme (0.14 U/mL) were added. The concentrations of NPs were adjusted to 200, 400, 600, and 800 ppm in PBS (pH 6.8). Acarbose was used as a positive control. The reaction time was set to 10 min at 37 °C with absorbance at 530 nm. A microtiter plate reader measured absorbance at 530 nm relative to a blank [29]. Equation (2) was employed to determine the % inhibition.

$$\text{\% Inhibition} = \frac{Abs^{bl} - Abs^{ss}}{Abs^{bl}} \times 100 \quad (2)$$

where Abs^{bl} is the absorbance of the blank solution and Abs^{ss} means the absorbance of the sample.

2.7. Statistical analysis

For the analysis of the results, a complete randomized design was employed for all the experiments. The antibacterial, antioxidant, and antidiabetic experiments were subjected to one-way ANOVA analysis. All the experiments were conducted in triplicate.

3. Results and discussion

3.1. X-ray diffraction

XRD is a crucial tool for analyzing the crystal structure of synthesized materials. It is often used to obtain detailed information on a material's crystalline structure, phase characteristics, lattice parameters, and grain structure [30]. Figure 1 shows the X-ray spectra of Ag_3O_4, chitosan-coated Ag_3O_4, and PEG–chitosan dually coated Ag_3O_4 synthesized by using the hydrothermal process. In the case of Ag_3O_4, the XRD spectrum presents diffraction peaks of Ag_3O_4 located at 2θ of 27.09°, 33.25°, 38.54°, 44.81°, and 54.90° and attributed to (110), (031), (022), (032), and (−202) planes, respectively. All the diffraction peaks correspond to the JCPDS Card # 00-077-1846, which indicates a cubic phase. However, the introduction of chitosan in the reaction disappears the diffraction peak at 27.09° and also transforms the intensity of the remaining peaks. Additionally, peak broadness is increased with chitosan coating, indicating the shift towards an amorphous phase. The crystallite size (D) is calculated by using Debye–Scherrer's formula (Equation (3)) [31].

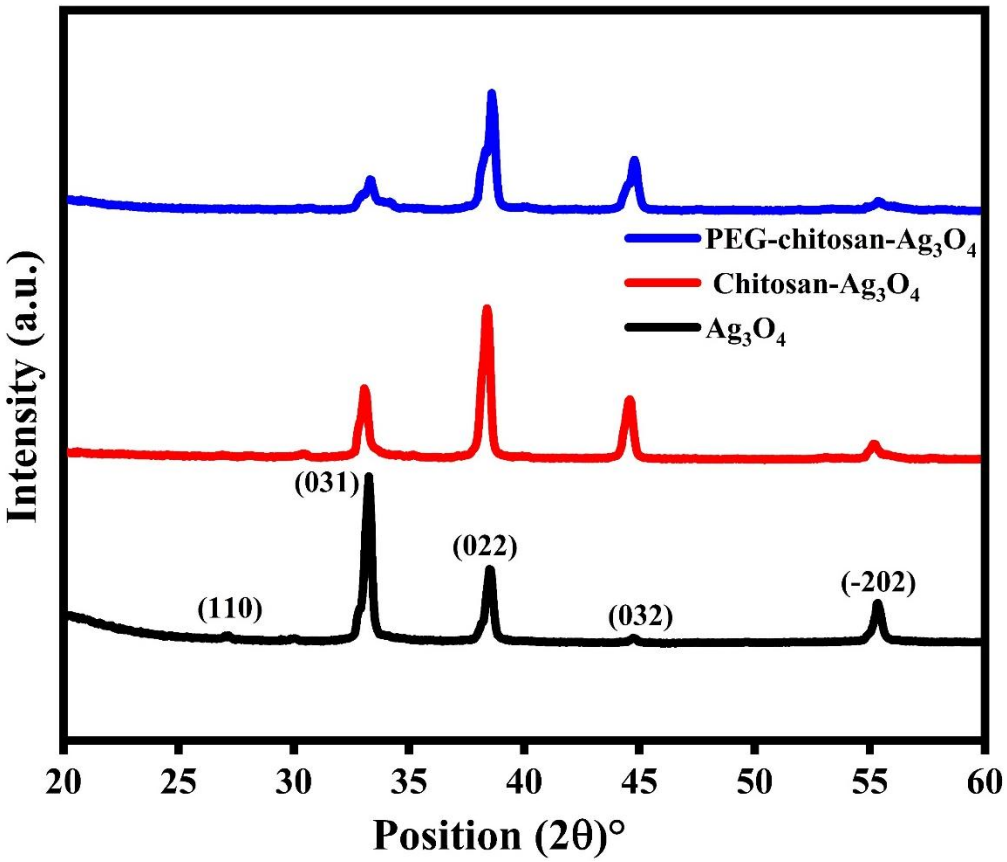

Figure 1. XRD patterns of hydrothermally synthesized Ag_3O_4, chitosan–Ag_3O_4, and PEG–chitosan–Ag_3O_4 nanomaterials.

$$D = \frac{K\lambda}{\beta \cos\theta} \tag{3}$$

where K = 0.9 is the shape factor, λ represents the wavelength of irradiated X-rays, β is the full width at half maximum, and θ is Bragg's angle. The crystallite size is determined as 49 nm for Ag_3O_4 which decreases to 25 nm (chitosan–Ag_3O_4), and 22 nm (PEG–chitosan Ag_3O_4) (Table 1). A combination of PEG and chitosan reduces the crystallite size of Ag_3O_4, indicating that polymers limit agglomeration during synthesis [4]. The decrease in size coincides with the bonding of polymer molecules to crystals, which hinders the further development of crystals and influences the

morphology, including structure, size, and size distribution of the nanomaterials [32]. The crystallite size is also calculated through the Williamson–Hall method which shows the same trend as observed in the case of Debye–Scherrer's formula. However, sizes calculated by the Williamson–Hall method are considerably less than Scherrer's method, indicating induced defects in the crystals that contract the crystallite size. This explanation is also supported by the calculation of strain and dislocation density which are higher for polymer-coated Ag_3O_4 NPs (Table 1).

Table 1. Structural parameters determined from XRD spectra of Ag_3O_4, and polymer-coated Ag_3O_4.

Sample Name	$D_{Scherrer}$	$D_{W.H}$	Strain	Dislocation density (lines/m^2)
Ag_3O_4	49 nm	28 nm	0.00025	9.58×10^{14}
Chitosan–Ag_3O_4	25 nm	17 nm	0.00072	1.56×10^{15}
PEG–chitosan Ag_3O_4	22 nm	10 nm	0.00221	2.32×10^{15}

The texture coefficient (TC_{hkl}) is calculated by Equation (4) to determine crystallite growth orientation.

$$\text{Texture coefficient (hkl)} = \frac{\left(\frac{I_{hkl}}{I_0\,(hkl)}\right)}{\left(\frac{1}{N}\right)\sum I(hkl)/I_0\,(hkl)} \quad (4)$$

The peak with the largest TC_{hkl} indicates the favored growth plane for the formation of crystals. For Ag_3O_4, the (110) plane has the highest TC_{hkl} value, showing a higher probability of crystal growth in the (110) orientation from the thermodynamic aspect. The polymer-functionalized Ag_3O_4 has a preferential growth direction along the (031) plane, as shown in Table 2.

Table 2. Texture coefficient value for Ag_3O_4, and polymer-coated Ag_3O_4.

(hkl)	Ag_3O_4	Chitosan–Ag_3O_4	PEG–chitosan–Ag_3O_4
(110)	4.39	-	-
(031)	0.31	3.82	3.59
(022)	0.02	0.06	0.05
(032)	0.23	0.07	0.03
(−212)	0.04	0.05	0.32

3.2. Scanning electron microscopy

The surface properties and nanoscale morphology of Ag_3O_4, chitosan–Ag_3O_4, and PEG–chitosan–Ag_3O_4 nanomaterials were examined using SEM. The low and high magnification SEM images of synthesized nanomaterials are shown in Figure 2(a–f). In the case of Ag_3O_4, spherical particles are observed with some aggregation and have a particle size of 75 ± 17 nm (Figure 2(a–b)). The chitosan–Ag_3O_4 nanomaterials, as shown in Figures 2(c,d), have spherical particles with a mean size of 35 ± 5 nm. The PEG–chitosan–Ag_3O_4 also presents an identical spherical shape; however, the particle size is considerably larger, i.e., 83 + 17 nm (Figure 2(e–f)). The observed change in particle size may be related to the combination structure of Ag_3O_4 and chitosan

coating with PEG, which controls the binding of additional atoms to the particles during the synthesis process [33].

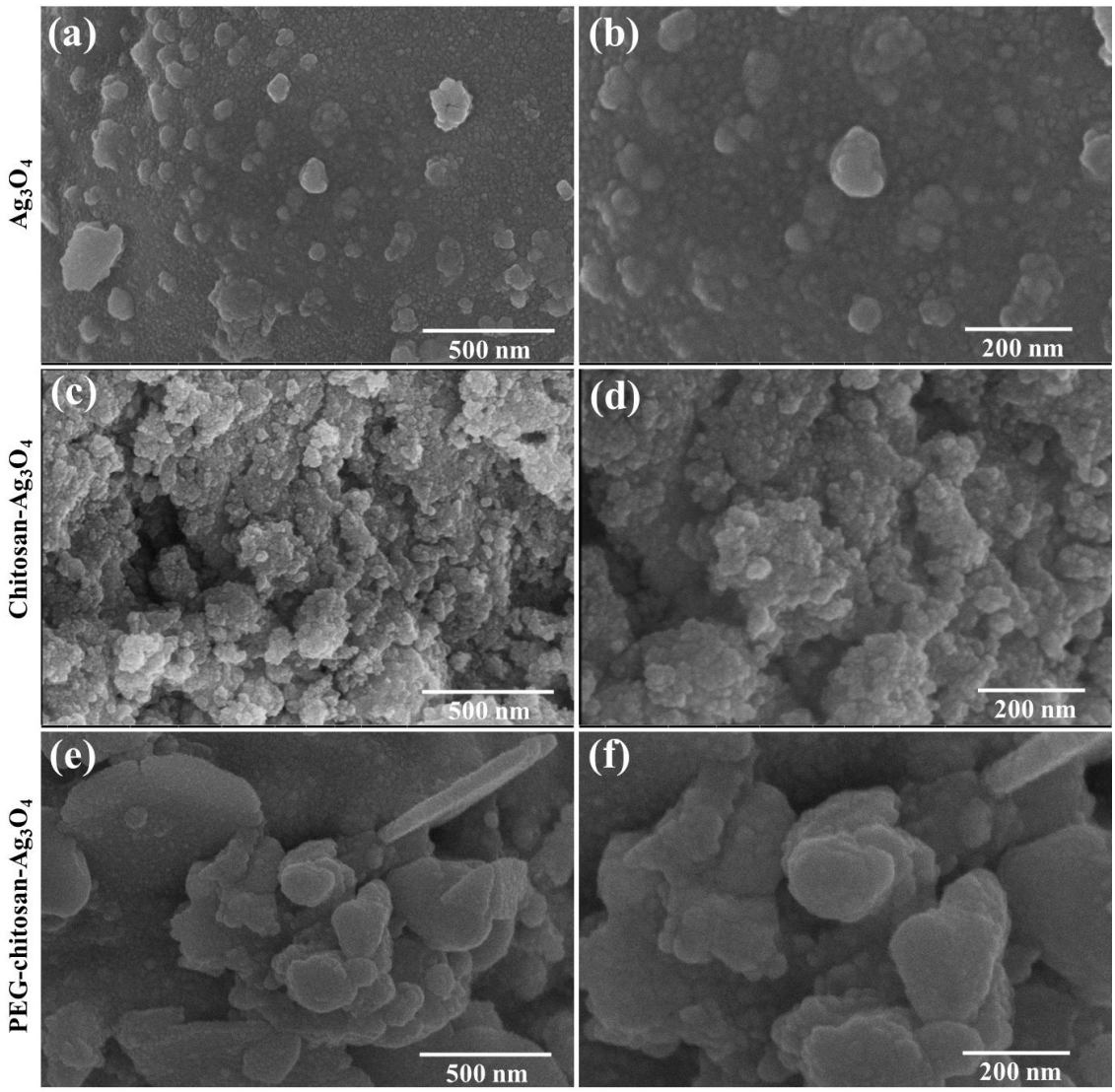

Figure 2. SEM images of (a–b) Ag_3O_4; (c–d) chitosan–Ag_3O_4; (e–f) PEG–chitosan Ag_3O_4 at low and high magnification.

3.3. UV–vis spectroscopy

UV–vis spectroscopy is used to evaluate the optical properties of Ag_3O_4-based nanomaterials, as shown in Figure 3(a,b). The absorption curve exhibits typical absorption in the wavelength range of 400–430 nm. Silver is a noble metal, and it undergoes absorption due to its surface plasmon resonance. A surface plasmon represents electromagnetic radiation confined to the surface of a metal and its interactions with the metal's free electrons. The surface plasmon resonance is a specific feature exhibited by metal NPs and cannot be found in the bulk form of the metal [34]. The optical band gap of Ag_3O_4 NPs is found to be 3.48 eV, as shown in Figure 3(b) [35]. But in the case of chitosan–Ag_3O_4 and PEG–chitosan–Ag_3O_4, the band gap is significantly decreased to 2.3 eV and 2.4 eV, respectively. The presence of chitosan and PEG in Ag_3O_4 may result in extra energy levels. These energy levels can decrease the energy required for electrons to transition from the valence band to the conduction band, thereby narrowing the band gap. This reduction in bandgap is linked with enhanced ROS generation, which ultimately improves the antibacterial properties of the materials [36].

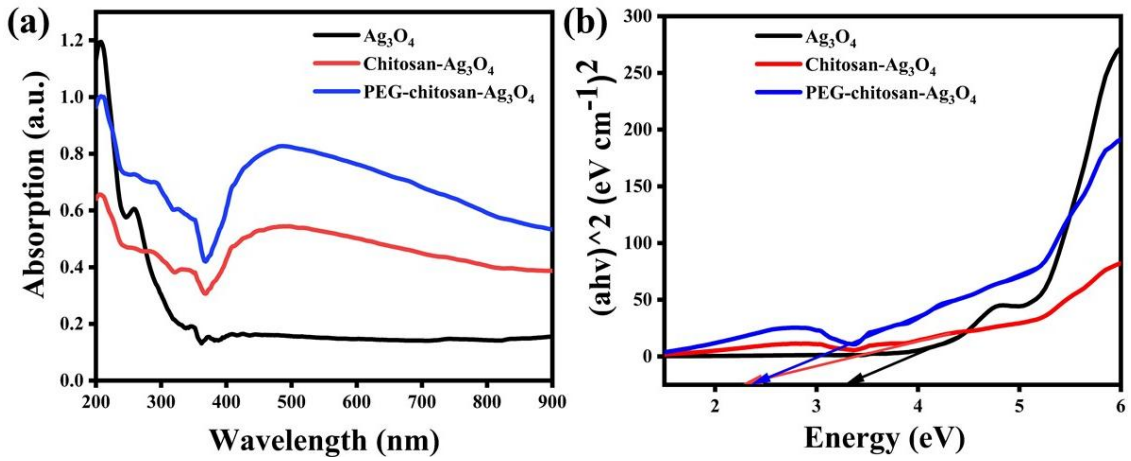

Figure 3. (a) UV-visible absorption curves; (b) Tauc's plot, of Ag_3O_4, chitosan–Ag_3O_4, and PEG–chitosan–Ag_3O_4.

3.4. Fourier transform infrared spectroscopy

FTIR is a useful technique for analyzing the functional groups, vibrational modes, and bond stretching characteristics on the surface of the produced Ag_3O_4 and its combination with chitosan and PEG. FTIR spectra are obtained in the range of 650–4000 cm^{-1} at room temperature (Figure 4). The band observed at a wave number of 829 cm^{-1} in Ag_3O_4 NPs is associated with the Ag-O bonding [37,38]. The peak at 1523 cm^{-1} in the case of Ag_3O_4 NPs coated with chitosan is due to the N-O stretching. The transmittance band at 1688 cm^{-1} corresponds to chitosan due to C≡N stretching [39]. The peaks located at 2000 cm^{-1} and 2112 cm^{-1} are attributed to C-H bending and C≡C stretching, respectively. The band at 2325 cm^{-1} belongs to the antisymmetric stretching mode of O=C=O stretching [40]. The transmittance band at 3731 cm^{-1} is related to the stretching of O-H bonds, indicating adsorbed water molecules [41].

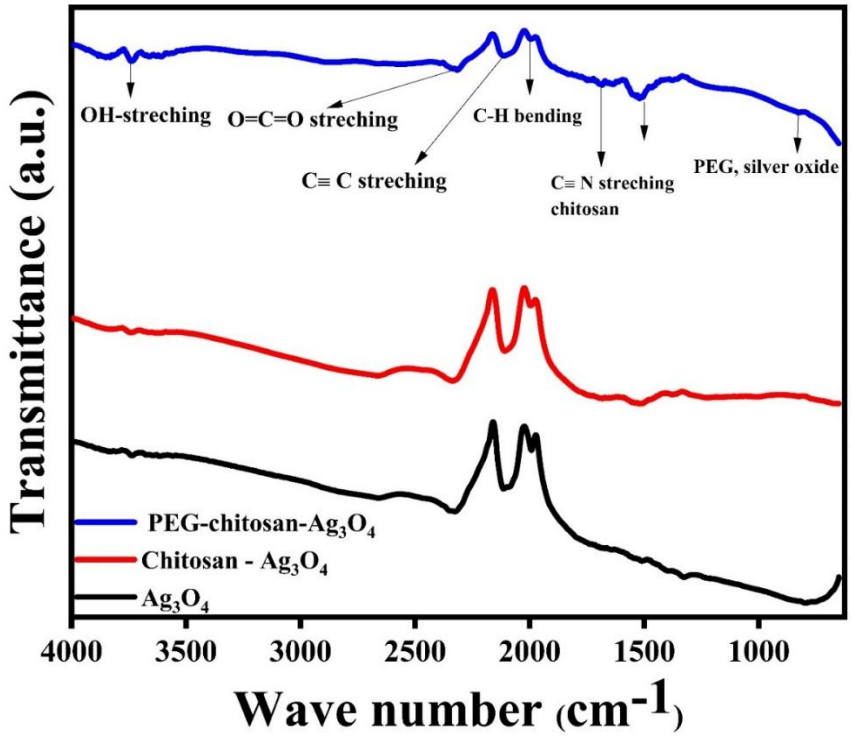

Figure 4. FTIR spectra of Ag_3O_4, chitosan-coated Ag_3O_4, and PEG–chitosan–Ag_3O_4 nanomaterials.

3.5. In vitro biological activity

3.5.1. Antibacterial properties

The antibacterial potential of Ag_3O_4 NPs against G+ and G− bacterial strains has been well-established over the years. The unique coordination environment of Ag^+ ions and O^{2-} ions in the crystal structure of Ag_3O_4 lays the foundation of the antibacterial properties [42]. Zones of inhibition (in mm) of pristine and chitosan-coated and PEG–chitosan-coated Ag_3O_4 NPs with chitosan and PEG are mentioned in Table 3 and evidenced by Figure 5. The smaller crystallite size (22 nm in the PEG–chitosan case) increases the surface area, thus enhancing the bacterial contact and ROS generation. Thereby, PEG–chitosan coating has further increased the antibacterial action of Ag_3O_4 NPs. The preferred growth orientation along the (031) plane in the case of polymer functionalized silver oxide NPs may have exposed more active facets for biological interactions. Chitosan coating gives a positive charge to the coated material due to its protonation ability [43]. This increases the strength of NPs' biological interaction with bacterial cells due to electrostatic interaction and ensures uniform dispersion of NPs in the biological medium [44,45]; consequently, the performance of Ag_3O_4 NPs improves. After the attachment to the bacterial cell, Ag_3O_4 NPs generate a significant quantity of ROS [46]. These ROS damage the cell walls of bacteria through oxidative stress [47]. Moreover, silver ions can destroy the electron transport chain; hence, the entire metabolism of the bacterial cell is disturbed [48]. These stress conditions are the major causes behind bacterial inhibition (Figure 6). However, in the case of PEG–chitosan Ag_3O_4 NPs, the antibacterial effect is further improved than chitosan coating. PEG and chitosan both possess intrinsic antibacterial properties [49,50]. After coating with Ag_3O_4 NPs, the antibacterial response is boosted by the synergistic effect of inorganic and organic phases.

Table 3. Zones of inhibition (ZOI) observed for bare and polymer-coated Ag_3O_4 NPs against *S. aureus* and *E. coli*.

Sample	Zone of Inhibition (mm)	
	S. aureus	***E. coli***
Ag_3O_4	09	10
Chitosan–Ag_3O_4	14	15
PEG–chitosan–Ag_3O_4	15	16
Ciprofloxacin (control)	32	34

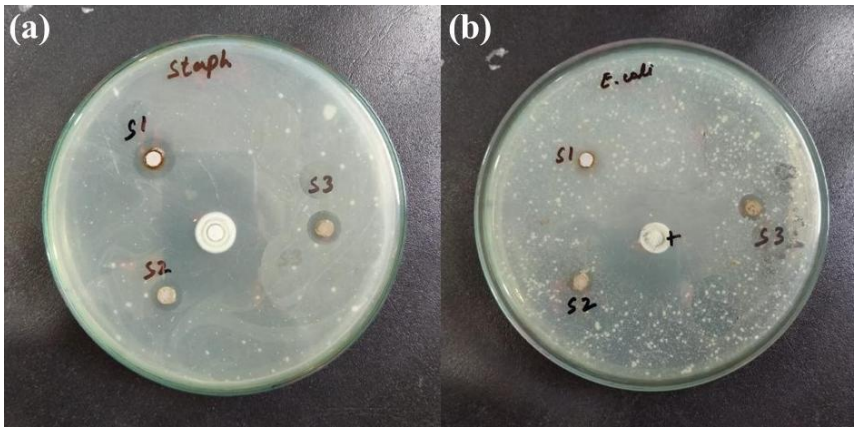

Figure 5. Zone of inhibition for pristine Ag_3O_4 (S1), chitosan–Ag_3O_4 (S2), and PEG–chitosan–Ag_3O_4 (S3) NPs against bacterial strains. (a) *Staphylococcus aureus*; (b) *Escherichia coli*.

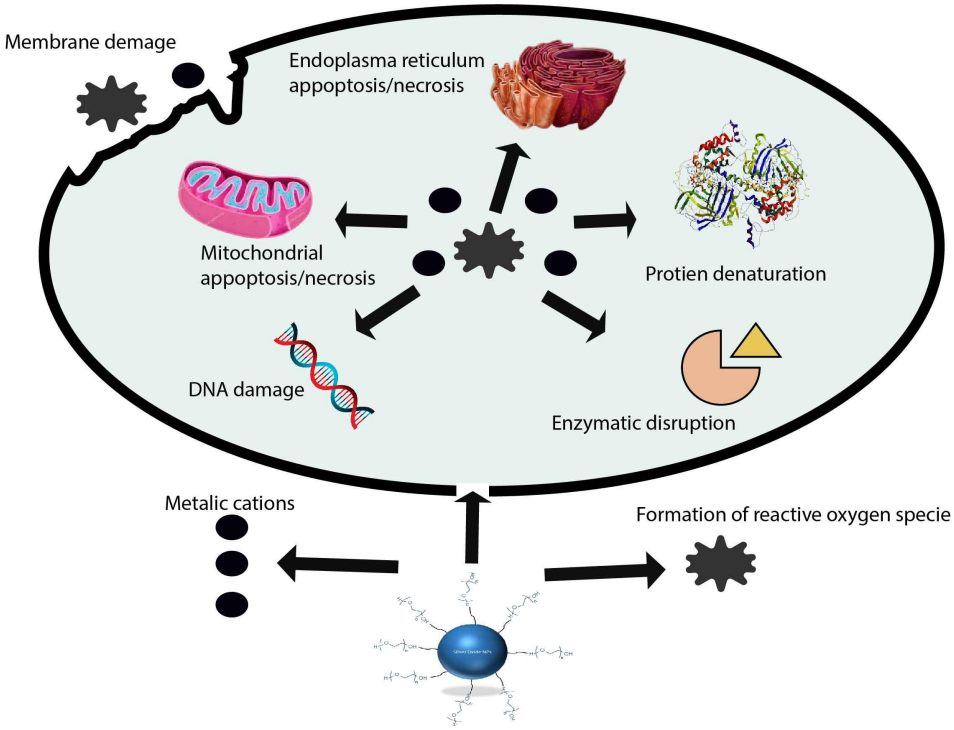

Figure 6. Antibacterial mechanism based on polymer-coated silver oxide NPs.

3.5.2. Antioxidant activity

Antioxidants are chemical substances that neutralize reactive species by inhibiting oxidation processes, thereby preventing cellular damage caused by excessive ROS generation. Natural antioxidants are highly demanded compounds due to their efficacy in regulating ROS-mediated pathogenesis of degenerative disorders, including cardiovascular and carcinogenesis diseases [51,52]. This approach serves to assess the antioxidant capacity in diverse foods, including juices, extracts, vegetables, and biosynthesized nanomaterials. It is a straightforward, cost-effective, and exceptionally sensitive methodology [53]. The DPPH assays are designed to assess the antioxidant activity of biomaterials, i.e., Ag_3O_4 and polymer-Ag_3O_4. The standard measure for antioxidant activity, referred to as ascorbic acid equivalents, comprises all of these compounds. Figure 7 illustrates that chitosan-coated Ag_3O_4 NPs' antioxidant capacity is significantly enhanced as compared to Ag_3O_4 and PEG–chitosan Ag_3O_4 NPs, with a maximum absorption wavelength at 520 nm. The reduced form of DPPH may donate an oxygen atom, causing the solution to lose its characteristic violet color [54]. The DPPH assay outcomes indicate that chitosan–Ag_3O_4 at 10 μg/mL exhibits the maximum radical scavenging activity of 38%. The lowest radical scavenging activity is measured as 8% for PEG–chitosan Ag_3O_4. The reduction in antioxidant activity after PEG addition can be attributed to the surface shielding effects and steric hindrance caused by the PEG chains. Cui et al. [55] discussed that the PEG coating might shield chitosan's active sites, resulting in a reduction of radical scavenging. This shows that PEG layer formation on chitosan reduces its antioxidant activity.

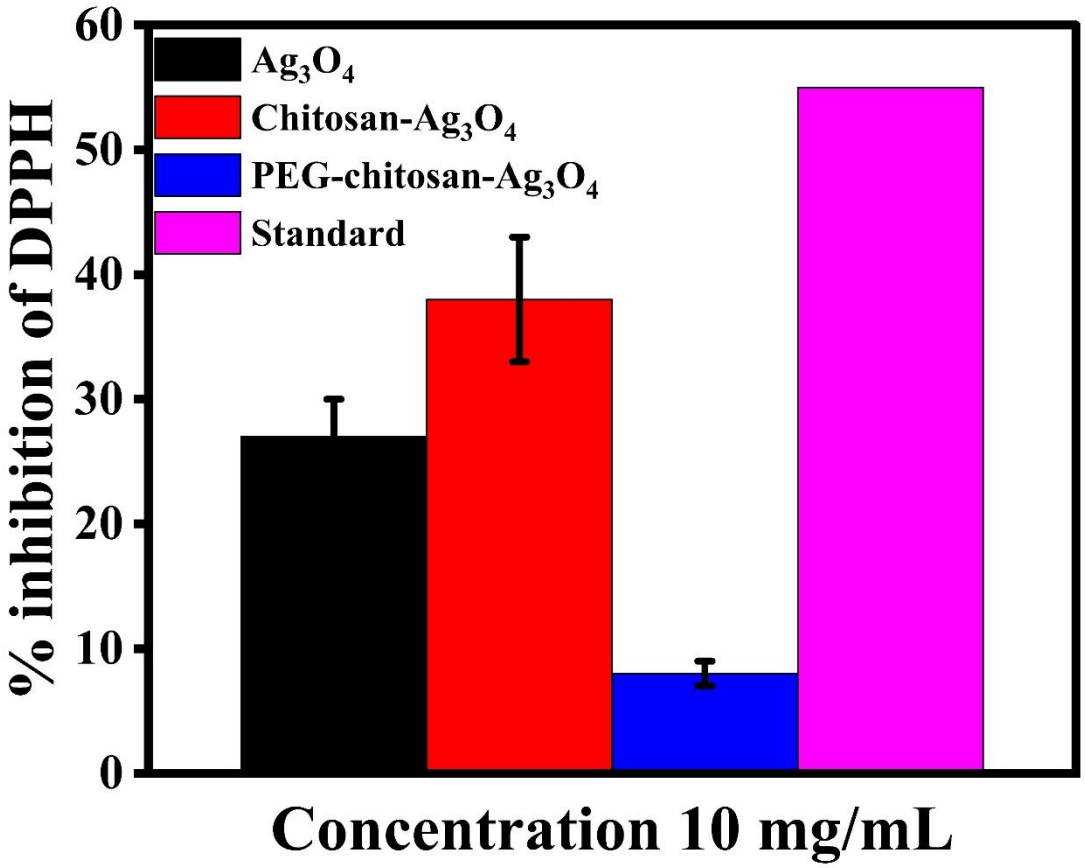

Figure 7. Antioxidant potential (% inhibition of DPPH) of Ag_3O_4, chitosan-coated Ag_3O_4, and PEG–chitosan–Ag_3O_4 NPs compared to the inhibition of ascorbic acid.

3.5.3. Antidiabetic analysis

Hyperglycemia occurs due to the insufficient capacity of the body to produce or respond to insulin. Insufficient insulin release in the human body results in diabetes mellitus, which causes the blood glucose level to rise [56]. Diabetes can be maintained artificially by injecting antidiabetic medications to control blood glucose levels. Postprandial hyperglycemia can be prevented by inhibiting enzymes in the intestines responsible for carbohydrate breakdown, with alpha-amylase being a specific target of certain drugs [57]. Various dosages (at dilution ranges from 200 ppm to 800 ppm) of synthesis formulations are employed on *in vitro* assays of alpha-amylase inhibition. The Ag_3O_4 exhibits a dose-dependent inhibitory outcome on alpha-amylase activity. The most significant inhibitory effect of Ag_3O_4 NPs and with polymers on alpha-amylase occurs at a concentration of 800 ppm, whereas the lowest inhibitory effect was noted at a value of 200 ppm (Figure 8). A comparison of materials characteristics and applications is provided in Table 4.

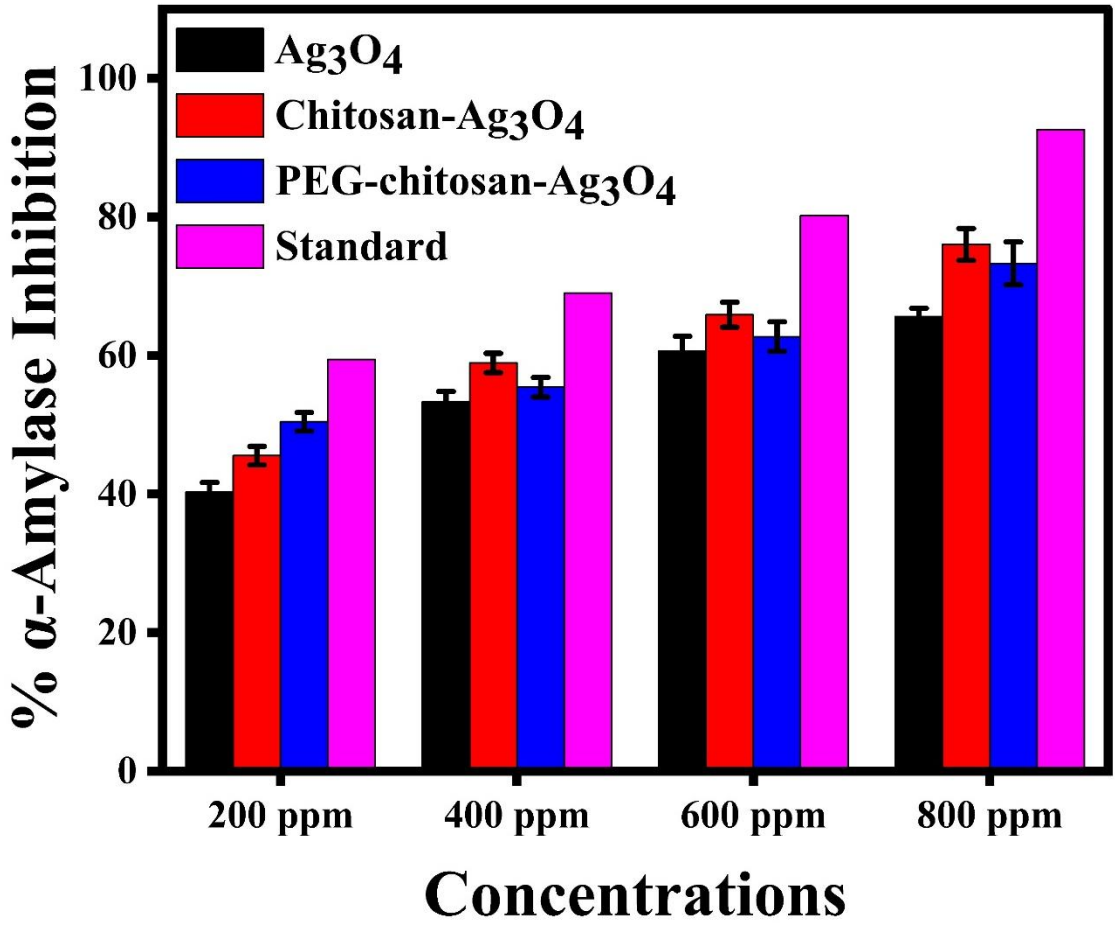

Figure 8. Percentage enzyme (alpha-amylase) inhibition ability of bare Ag_3O_4, chitosan-coated Ag_3O_4, and PEG–chitosan-coated Ag_3O_4 nanomaterials.

Table 4. Comparison of structural, optical, and biological properties of pristine, chitosan-coated, and PEG–chitosan-coated Ag_3O_4 nanoparticles.

Parameter	Ag_3O_4 NPs	Chitosan–Ag_3O_4 NPs	PEG–Chitosan–Ag_3O_4 NPs	Significance
Crystallite size (XRD)	49 nm	25 nm	22 nm	Reduced size enhances surface area/reactivity
Bandgap (eV)	3.48	2.30	2.40	Lower bandgap promotes ROS generation
ZOI against *S. aureus*	9	14	15	Dual coating shows maximal antibacterial synergy
ZOI against *E. coli*	10	15	16	Dual coating shows maximal antibacterial synergy
DPPH scavenging (%)	28	38	8	Chitosan alone favors antioxidant activity
α-amylase inhibition % (800 ppm)	Good	Best	Best (with minute difference)	PEG–chitosan optimizes antidiabetic potential

4. Limitations

Although the current study presents the improved multifunctional biological efficacy of PEG–chitosan dully coated Ag_3O_4 NPs, certain limitations should be taken into account while interpreting the findings. Firstly, all the biological trials are performed using *in vitro* models, including antibacterial, antioxidant, and enzyme inhibition assays. The results of these assays demonstrate valuable preliminary evidence of biological activity; however, they do not cover the complexity of the *in vivo* physiological conditions. Sometimes, during *in vivo* trials, the behavior of NPs is altered after interacting with biological fluids and causing a change in immune responses and metabolic pathways. Secondly, toxicity and hemocompatibility assays for mammalian cells are not included in this study. Even though PEG and chitosan are generally recognized as biocompatible polymers, detailed biosafety profiling is necessary to support future clinical translation of the PEG–chitosan-coated Ag_3O_4 NPs. Thirdly, the antibacterial potential of the nanomaterials is evaluated by using the agar well diffusion test, which primarily offers diffusion-dependent bacterial inhibition and does not confer quantitative bactericidal information, e.g., MIC, MBC, or biofilm inhibition percentage. Incorporation of such analyses would enhance mechanistic interpretation. Lastly, the long-term colloidal stability and release kinetics of Ag ions in biological media have not been studied, which may affect therapeutic efficacy. These limitations define a clear direction for future investigations and do not detract from the significance of the present study.

5. Conclusion

The present study successfully synthesized dually coated Ag_3O_4 NPs via the hydrothermal method. The dual polymer functionalization reduced the crystallite size to 22 nm and narrowed the optical band gap to 2.3 eV, which enhanced the reactive surface area and electron transfer capability of Ag_3O_4 NPs. The dually coated nanomaterials showed significant antibacterial activity against both Gram-positive and Gram-negative bacteria. Chitosan functionalization demonstrated superior

antioxidant potential (38% DPPH scavenging), while PEG–chitosan functionalization exhibited the highest α-amylase inhibition potential of Ag_3O_4 NPs. These findings confirmed the synergistic integration of PEG and chitosan on the surface of Ag_3O_4 NPs that optimizes the multifunctional biological efficacy, making them potential candidates for advanced biomedical applications in combatting bacterial infections, oxidative stress management, and diabetes-related pathways. The present study was conducted mainly on *in vitro* models. It lacks toxicity profiling, and MIC/MBC data were not observed for *S. aureus* and *E. coli*. This research work can be extended for *in vivo* biocompatibility studies, mechanistic biofilm assays, and pharmacokinetic evaluation of Ag^+ release.

Acknowledgments: The authors thank all the peer reviewers for their opinions and suggestions.

AI declaration: No AI tool was used in the writing of this manuscript.

Availability of Data and Materials: The datasets used and analyzed during the current study are available from the corresponding author on reasonable request.

Funding: This research received no external funding.

Author Contributions: SI and AB conducted experimental work and wrote the initial draft. MKA and YJ designed the experiment and revised the manuscript. RA and MA performed biological experiments. SFBF critically revised the manuscript. All authors contributed to the critical revision of the manuscript for important intellectual content. All authors read and approved the final manuscript. All authors have participated sufficiently in the work and agreed to be accountable for all aspects of the work.

Conflicts of Interest: The author declare no conflict of interest.

References

1. Smirnova, V.V.; Chausov, D.N.; Serov, D.A.; et al. A Novel Biodegradable Composite Polymer Material Based on PLGA and Silver Oxide Nanoparticles with Unique Physicochemical Properties and Biocompatibility with Mammalian Cells. *Materials* 2021, 14, 6915. https://doi.org/10.3390/ma14226915
2. Chausov, D.N.; Smirnova, V.V.; Burmistrov, D.E.; et al. Synthesis of a Novel, Biocompatible and Bacteriostatic Borosiloxane Composition with Silver Oxide Nanoparticles. *Materials* 2022, 15, 527. https://doi.org/10.3390/ma15020527
3. Mohanta, Y.K.; Biswas, K.; Jena, S.K.; et al. Anti-biofilm and Antibacterial Activities of Silver Nanoparticles Synthesized by the Reducing Activity of Phytoconstituents Present in the Indian Medicinal Plants. *Frontiers in Microbiology* 2020, 11, 1143. https://doi.org/10.3389/fmicb.2020.01143
4. Abbas, M.K.; Javed, Y.; Jamil, Y.; et al. Polyethylene glycol dictates the therapeutic response (anticancer and wound healing) of silver oxide nanomaterials. *Polymers for Advanced Technologies* 2023, 34, 2606–2619. https://doi.org/10.1002/pat.6076
5. Cao, Y.H.; Cai, W.J.; He, X.W.; et al. A review of advances & potential of applying nanomaterials for biofilm inhibition. *Npj Clean Water* 2024, 7, 131. https://doi.org/10.1038/s41545-024-00423-5
6. More, P.R.; Pandit, S.; Filippis, A.D.; et al. Silver Nanoparticles: Bactericidal and Mechanistic Approach against Drug Resistant Pathogens. *Microorganisms* 2023, 11, 369. https://doi.org/10.3390/microorganisms11020369
7. Krystosiak, P.; Tomaszewski, W.; Megiel, E. High-density polystyrene-grafted silver nanoparticles and their use in the preparation of nanocomposites with antibacterial properties. *Journal of Colloid and Interface Science* 2017, 498, 9–21. https://doi.org/10.1016/j.jcis.2017.03.041
8. Tran, Q.H.; Nguyen, V.Q.; Le, A.T. Silver nanoparticles: synthesis, properties, toxicology, applications and perspectives. *Advances in Natural Sciences: Nanoscience and Nanotechnology* 2013, 4, 033001. https://doi.org/10.1088/2043-6254/aad12b
9. Lyutakov, O.; Kalachyova, Y.; Solovyev, A.; et al. One-step preparation of antimicrobial silver nanoparticles in polymer matrix. *Journal of Nanoparticle Research* 2015, 17, 1–11. https://doi.org/10.1007/s11051-015-2935-3

10. Tripathi, S.; Mehrotra, G.K.; Dutta, P.K. Chitosan–silver oxide nanocomposite film: Preparation and antimicrobial activity. *Bulletin of Materials Science* 2011, 34, 29–35. https://doi.org/10.1007/s12034-011-0032-5
11. Hu Z, Zhang J, Chan WL, et al. Synthesis and characterization of nanostructured materials. In: *MRS Online Proceedings Library, Proceedings of the Materials Research Society Conference*; April 17 – 21, 2006; San Francisco, USA. Materials Research Society; 2006. 987: 45 – 50
12. Shi, L.W.; Zhang, J.Q.; Zhao, M.; et al. Effects of polyethylene glycol on the surface of nanoparticles for targeted drug delivery. *Nanoscale* 2021, 13, 10748–10764. https://doi.org/10.1039/D1NR02065J
13. Rinaudo, M. Chitin and chitosan: Properties and applications. Progress in polymer science 2006, 31, 603-632. https://doi.org/10.1016/j.progpolymsci.2006.06.001
14. Muxika, A.; Etxabide, A.; Uranga, J.; et al. Chitosan as a bioactive polymer: Processing, properties and applications. *International Journal of Biological Macromolecules* 2017, 105, 1358–1368. https://doi.org/10.1016/j.ijbiomac.2017.07.087
15. Peng, Y.; Song, C.; Yang, C.; et al. Low molecular weight chitosan-coated silver nanoparticles are effective for the treatment of MRSA-infected wounds. *International Journal of Nanomedicine* 2017, 12, 295–304. https://doi.org/10.2147/IJN.S122357
16. Laib, I.; Mohammed, H.A.; Laouini, S.E.; et al. Cutting-edge nanotherapeutics: silver nanoparticles loaded with ciprofloxacin for powerful antidiabetic, antioxidant, anti-inflammatory, and antibiotic action against resistant pathogenic bacteria. *International Journal of Food Science and Technology* 2025, 60, vvaf024. https://doi.org/10.1093/ijfood/vvaf024
17. Qadeer, B.; Khan, M.A.; Tariq, H.; et al. PEGylation of silver nanoparticles via Berginia Ciliata aqueous extract for biological applications. *Emergent Materials* 2024, 7, 1657–1673. https://doi.org/10.1007/s42247-024-00727-9
18. Batool, A.; Aisida, S.O.; Javed, R.; et al. PEG Capped $Nix Co_{1-x} Fe_2O_4$ Nanocomposites: Microstructural, Morphological, Optical, Magnetic, Antimicrobial, and Photodegradable Properties. *BioNanoScience* 2023, 13, 1–12. https://doi.org/10.1007/s12668-023-01064-7
19. Rajkumar, M.; Davis Presley, S.I.; Girigoswami, K.; et al. Development of Polyethylene Glycol–Coated CuO Nanocomposites for Enhanced Antioxidant, Antibacterial, Biocompatible and Anticancer Activities. *Biomedical Materials & Devices* 2025, 3, 1–27. https://doi.org/10.1007/s44174-025-00623-8
20. Bahramikia, S.; Ardestani, A.; Yazdanparast, R. Protective effects of four Iranian medicinal plants against free radical-mediated protein oxidation. *Food Chemistry* 2009, 115, 37–42. https://doi.org/10.1016/j.foodchem.2008.11.054
21. Liu, J.; Wang, C.N.; Wang, Z.Z.; et al. The antioxidant and free-radical scavenging activities of extract and fractions from corn silk (*Zea mays* L.) and related flavone glycosides. *Food chemistry* 2011, 126, 261–269. https://doi.org/10.1016/j.foodchem.2010.11.014
22. Yan, D.Z.; Li, Y.Z.; Liu, Y.L.; et al. Antimicrobial Properties of Chitosan and Chitosan Derivatives in the Treatment of Enteric Infections. *Molecules* 2021, 26, 7136. https://doi.org/10.3390/molecules26237136
23. Amin, M.K.; Boateng, J.S. Enhancing Stability and Mucoadhesive Properties of Chitosan Nanoparticles by Surface Modification with Sodium Alginate and Polyethylene Glycol for Potential Oral Mucosa Vaccine Delivery. *Marine Drugs* 2022, 20, 156. https://doi.org/10.3390/md20030156
24. Fahmy, S.A.; Ramzy, A.; El Samaloty, N.M.; et al. PEGylated Chitosan Nanoparticles Loaded with Betaine and Nedaplatin Hamper Breast Cancer: In Vitro and In Vivo Studies. *ACS Omega* 2023, 8, 41485–41494. https://doi.org/10.1021/acsomega.3c05359
25. Adschiri, T.; Hakuta, Y.; Arai, K. Hydrothermal Synthesis of Metal Oxide Fine Particles at Supercritical Conditions. *Industrial & Engineering Chemistry Research* 2000, 39, 4901–4907. https://doi.org/10.1021/ie0003279
26. Adschiri, T.; Hakuta, Y.; Sue, K.; et al. Hydrothermal Synthesis of Metal Oxide Nanoparticles at Supercritical Conditions. *Journal of Nanoparticle Research* 2001, 3, 227–235. https://doi.org/10.1023/A:1017541705569
27. Mustafa, I.; Faisal, M.N.; Hussain, G.; et al. Efficacy of *Euphorbia helioscopia* in context to a possible connection between antioxidant and antidiabetic activities: a comparative study of different extracts. *BMC Complementary Medicine and Therapies* 2021, 21, 62. https://doi.org/10.1186/s12906-021-03237-x

28. Zohra, T.; Ovais, M.; Khalil, A.T.; et al. Extraction optimization, total phenolic, flavonoid contents, HPLC-DAD analysis and diverse pharmacological evaluations of *Dysphania ambrosioides* (L.) Mosyakin & Clemants. *Natural Product Research* 2019, 33, 136–142. https://doi.org/10.1080/14786419.2018.1437428
29. Unuofin, J.O.; Otunola, G.A.; Afolayan, A.J. *In vitro* α-amylase, α-glucosidase, lipase inhibitory and cytotoxic activities of tuber extracts of *Kedrostis africana* (L.) Cogn. *Heliyon* 2018, 4, e00810. https://doi.org/10.1016/j.heliyon.2018.e00810
30. Mourdikoudis, S.; Pallares, R.M.; Thanh, N.T.K. Characterization techniques for nanoparticles: comparison and complementarity upon studying nanoparticle properties. *Nanoscale* 2018, 10, 12871–12934. https://doi.org/10.1039/C8NR02278J
31. Pandya, S.G.; Corbett, J.P.; Jadwisienczak, W.M.; et al. Structural characterization and X-ray analysis by Williamson–Hall method for Erbium doped Aluminum Nitride nanoparticles, synthesized using inert gas condensation technique. *Physica E: Low-dimensional Systems and Nanostructures* 2016, 79, 98–102. https://doi.org/10.1016/j.physe.2015.12.013
32. Dadashi, S.; Poursalehi, R.; Delavari H.H. In situ PEGylation of Bi nanoparticles prepared via pulsed Nd:YAG laser ablation in low molecular weight PEG: a potential X-ray CT imaging contrast agent. *Computer Methods in Biomechanics and Biomedical Engineering: Imaging & Visualization* 2019, 7, 420-427. https://doi.org/10.1080/21681163.2018.1452634
33. Manson, J.; Kumar, D.; Meenan, B.J.; et al. Polyethylene glycol functionalized gold nanoparticles: the influence of capping density on stability in various media. *Gold bulletin* 2011, 44, 99–105. https://doi.org/10.1007/s13404-011-0015-8
34. Zeng, S.W.; Yu, X.; Law, W.C.; et al. Size dependence of Au NP-enhanced surface plasmon resonance based on differential phase measurement. *Sensors and Actuators B: Chemical* 2013, 176, 1128–1133. https://doi.org/10.1016/j.snb.2012.09.073
35. Al-Sarraj, A.; Saoud, K.M.; Elmel, A.; et al. Optoelectronic properties of highly porous silver oxide thin film. *SN Applied Sciences* 2021, 3, 1–13. https://doi.org/10.1007/s42452-020-04091-1
36. Shafiee, A.; Ghadiri, E.; Kassis, J.; et al. Energy Band Gap Investigation of Biomaterials: A Comprehensive Material Approach for Biocompatibility of Medical Electronic Devices. *Micromachines* 2020, 11, 105. https://doi.org/10.3390/mi11010105
37. Basta, A.H.; Lotfy, V.F.; Mahmoud, K.; et al. Synthesis and evaluation of protein-based biopolymer in production of silver nanoparticles as bioactive compound versus carbohydrates-based biopolymers. *Royal Society Open Science* 2020, 7, 200928. https://doi.org/10.1098/rsos.200928
38. Cai, M.T.; Zhang, J.X.; Chen, Y.W.; et al. Preparation and characterization of chitosan composite membranes crosslinked by carboxyl-capped poly(ethylene glycol). *Chinese Journal of Polymer Science* 2014, 32, 236–244. https://doi.org/10.1007/s10118-014-1373-5
39. Rahimi, S.; Khoee, S.; Ghandi, M. Preparation and characterization of rod-like chitosan–quinoline nanoparticles as pH-responsive nanocarriers for quercetin delivery. *International Journal of Biological Macromolecules* 2019, 128, 279–289. https://doi.org/10.1016/j.ijbiomac.2019.01.137
40. Moafi, H.F.; Ansari, R.; Ostovar, F. Ag_2O/Sawdust nanocomposite as an efficient adsorbent for removal of hexavalent chromium ions from aqueous solutions. *Journal of Materials and Environmental Science* 2016, 7, 2051–2068. https://www.jmaterenvironsci.com/Document/vol7/vol7_N6/220-JMES-2015-Moafi.pdf
41. El-Sharnouby, M.; Askary, A.E.; Awwad, N.S.; et al. Enhanced Electrical Conductivity and Dielectric Performance of Ternary Nanocomposite Film of PEMA/PS/Silver NPs Synthesized by Laser Ablation. *Journal of Inorganic and Organometallic Polymers and Materials* 2022, 32, 2269–2278. https://doi.org/10.1007/s10904-022-02286-0
42. Minhas, L.A.; Kaleem, M.; Jabeen, A.; et al. Synthesis of Silver Oxide Nanoparticles: A Novel Approach for Antimicrobial Properties and Biomedical Performance, Featuring Nodularia haraviana from the Cholistan Desert. *Microorganisms* 2023, 11, 2544. https://doi.org/10.3390/microorganisms11102544
43. Frank, L.A.; Onzi, G.R.; Morawski, A.S.; et al. Chitosan as a coating material for nanoparticles intended for biomedical applications. *Reactive and Functional Polymers* 2020, 147, 104459. https://doi.org/10.1016/j.reactfunctpolym.2019.104459
44. Shoueir, K.R.; El-Desouky, N.; Rashad, M.M.; et al. Chitosan based-nanoparticles and nanocapsules: Overview, physicochemical features, applications of a nanofibrous scaffold, and bioprinting. *International Journal of Biological Macromolecules* 2021, 167, 1176–1197. https://doi.org/10.1016/j.ijbiomac.2020.11.072

45. Schubert, J.; Chanana, M. Coating Matters: Review on Colloidal Stability of Nanoparticles with Biocompatible Coatings in Biological Media, Living Cells and Organisms. *Current Medicinal Chemistry* 2018, 25, 4553–4586. https://doi.org/10.2174/0929867325666180601101859
46. Flores-López, L.Z.; Espinoza-Gómez, H.; Somanathan, R. Silver nanoparticles: Electron transfer, reactive oxygen species, oxidative stress, beneficial and toxicological effects. Mini review. *Journal of Applied Toxicology* 2019, 39, 16–26. https://doi.org/10.1002/jat.3654
47. Cheng, J.H.; Lv, X.Y.; Pan, Y.Y.; et al. Foodborne bacterial stress responses to exogenous reactive oxygen species (ROS) induced by cold plasma treatments. *Trends in Food Science & Technology* 2020, 103, 239–247. https://doi.org/10.1016/j.tifs.2020.07.022
48. Wang, G.M.; Jin, W.H.; Qasim, A.M.; et al. Antibacterial effects of titanium embedded with silver nanoparticles based on electron-transfer-induced reactive oxygen species. *Biomaterials* 2017, 124, 25–34. https://doi.org/10.1016/j.biomaterials.2017.01.028
49. Ardean, C.; Davidescu, C.M.; Nemeş, N.S.; et al. Factors Influencing the Antibacterial Activity of Chitosan and Chitosan Modified by Functionalization. *International Journal of Molecular Sciences* 2021, 22, 7449. https://doi.org/10.3390/ijms22147449
50. Ragaseema, V.M.; Unnikrishnan, S.; Krishnan, V.K.; et al. The antithrombotic and antimicrobial properties of PEG-protected silver nanoparticle coated surfaces. *Biomaterials* 2012, 33, 3083–3092. https://doi.org/10.1016/j.biomaterials.2012.01.005
51. Nagajyothi, P.C.; Cha, S.J.; Yang, I.J.; et al. Antioxidant and anti-inflammatory activities of zinc oxide nanoparticles synthesized using *Polygala tenuifolia* root extract. *Journal of Photochemistry and Photobiology B: Biology* 2015, 146, 10–17. https://doi.org/10.1016/j.jphotobiol.2015.02.008
52. Gupta, R.; Das, N.; Singh, M. Fabrication and surface characterisation of c-ZnO loaded TTDMM dendrimer nanocomposites for biological applications. *Applied Surface Science* 2019, 484, 781–796. https://doi.org/10.1016/j.apsusc.2019.04.136
53. Sowndhararajan, K.; Joseph, J.M.; Manian, S. Antioxidant and Free Radical Scavenging Activities of Indian *Acacias: Acacia Leucophloea* (Roxb.) Willd., *Acacia Ferruginea* Dc., *Acacia Dealbata* Link. and *Acacia Pennata* (L.) Willd. *International Journal of Food Properties* 2013, 16, 1717–1729. https://doi.org/10.1080/10942912.2011.604895
54. Muthukumar, H.; Palanirajan, S.K.; Shanmugam, M.K.; et al. Photocatalytic degradation of caffeine and *E. coli* inactivation using silver oxide nanoparticles obtained by a facile green co-reduction method. *Clean Technologies and Environmental Policy* 2022, 24, 1087–1098. https://doi.org/10.1007/s10098-021-02135-7
55. Cui, L.; Tang, C.; Yin, C. Effects of quaternization and PEGylation on the biocompatibility, enzymatic degradability and antioxidant activity of chitosan derivatives. *Carbohydrate Polymers* 2012, 87, 2505–2511. https://doi.org/10.1016/j.carbpol.2011.11.030
56. Al-Ishaq, R.K.; Abotaleb, M.; Kubatka, P.; et al. Flavonoids and Their Anti-Diabetic Effects: Cellular Mechanisms and Effects to Improve Blood Sugar Levels. *Biomolecules* 2019, 9, 430. https://doi.org/10.3390/biom9090430
57. Nair, S.S.; Kavrekar, V.; Mishra, A. In vitro studies on alpha amylase and alpha glucosidase inhibitory activities of selected plant extracts. *European Journal of Experimental Biology* 2013, 3, 128–132. https://www.researchgate.net/profile/Mabrur-Mabrur/post/alpha_amylase_assay/attachment/5ca4822fcfe4a7df4ae533de/AS%3A743539768045568%401554285103167/download/.pdf